FUNDAMENTALS & APPLICATIONS

CHEMELECTROCHEM

ANALYSIS & CATALYSIS, BIO & NANO, ENERGY & MORE

Accepted Article

Title: Common Battery Anode Testing Protocols Are Not Suitable for New Combined Alloying and Conversion Materials

Authors: Gerard Bree, Hugh Geaney, and Kevin Ryan

To be cited as: *ChemElectroChem* 10.1002/celc.201800990

Link to VoR: http://dx.doi.org/10.1002/celc.201800990

A Journal of

ChemPubSoc Europe

WILEY-VCH

www.chemelectrochem.org

10.1002/celc.201800990

Common Battery Anode Testing Protocols Are Not Suitable for New Combined Alloying and Conversion Materials

*Gerard Bree, Hugh Geaney, and Kevin M. Ryan**

Bernal Institute, University of Limerick, Limerick V94 T9PX, Ireland

ABSTRACT: Here we report an interesting observation on anode materials for lithium ion batteries that undergo combined conversion and alloying lithiation processes during cycling (CAMs). These materials are generating interest as low cost and high capacity alternatives to graphite. We find that common testing protocols (CTPs) are unsuitable for assessment of CAMs due to their distinct multi-step lithiation characteristics. CTPs involve reporting total gravimetric capacity in a half cell configuration alone (opposite Li foil), without individual analysis of each process; energy density and the problems associated with wide discharge voltages are not addressed. Through isolating the individual lithiation processes of a model system (Cu_2ZnSnS_4), we determine that the conversion processes are highly unstable, whereas the alloying processes exhibit remarkable capacity retention. We demonstrate that inclusion of the conversion processes in cycling actually reduced full cell energy density when compared with alloying alone. This indicates that CTPs may well underestimate the stability of CAMs. It is apparent that the true advantage of CAMs lies in the synergistic combination of the capacity of the alloying portion, and the stability provided by the uncycling Li_2S buffer material. Finally, we prescribe a set of testing protocols for a meaningful assessment of new CAMs.

Keywords: Battery Testing, Lithium-Ion Battery, Anode, CZTS, Lithiation Mechanism, Conversion, Alloying

Introduction

The increasing demand for higher capacity rechargeable batteries has brought about widespread study of new, higher performance anode materials. Potentially offering an order of magnitude increase in gravimetric capacity over commercially used intercalation-based graphite, these new materials are typically based on either conversion or alloying lithiation processes.[1–4] Alloying materials can offer very high theoretical lithiation capacities (e.g. 3,579 mAh g^{-1} and 994 mAh g^{-1} for Si[5] and Sn,[6] respectively) when compared with graphite (372 mAh g^{-1}).[7] Pure conversion materials typically offer lower capacities (e.g. 609 mAh g^{-1} for FeS[8] or 560 mAh g^{-1} for CuS[9]), but still provide a significant advantage over graphite. Despite these advantages, stability problems (pulverization/delamination in the case of alloying,[10,11] and poor electrode conductivity/voltage hysteresis in the case of conversion[3]) have, to date, prevented the widespread adoption of these pure mode materials. Recently, CAMs have emerged as potential next generation electrode materials, offering a path towards overcoming these individual limitations through synergistic interactions.[12–19] The most common and simple form of this material type is a binary metal/metalloid chalcogenide (e.g. ZnS, SnS_x, GeS), in which the metal/metalloid itself is active towards Li. The lithiation process of these materials proceeds with an initial conversion-mode formation of Li_2S, followed by formation of Li-metal alloys.

$$MS_x + 2xLi \rightarrow xLi_2S + M$$

$$M + yLi \rightarrow Li_yM$$

In the majority of reported studies of binary sulfides, the conversion step was irreversible.[20–25] Therefore, the inclusion of additional metals in the active material (typically Cu, forming ternary/quaternary sulfides) has been proposed to ensure reversible conversion and alloying modes are maintained under extended cycling. It has also been proposed that these ternary/quaternary systems provide even greater accommodation of volume expansion and enhanced conductivity when compared with binary analogues.[14,19] Materials based on this formulation, such as $CuSnS_3$,[14,19] Cu_3BiS_3,[26] $CuSbS_2$,[27,28] CuInZnS[29] and Cu_2ZnSnS_4[30–32] have demonstrated multiple reversible lithiation steps, with measured capacities up to 1,400 mAh g^{-1}.[30]

The combination of the two modes in a single material typically offers enhanced theoretical capacity.[20] Additionally, a synergistic effect arises from the Li_2S acting as a buffer/host preventing material agglomeration/loss during expansion in the alloying stage,[12,19,23] whereas the inclusion of the alloying stage typically increases capacity while lowering the average voltage vs Li/Li^+ (thereby providing greater overall energy density).[12]

However, further analysis of these reports indicate that several outstanding issues remain. An often overlooked facet is that the unique, multi-modal nature of the lithiation mechanism of CAMs requires testing protocols distinct from that of materials in which lithiation occurs through a single mode (such as graphite/Si/Ge). CTPs typically report the gravimetric capacity (in mAh g^{-1}) over a wide voltage range as the headline figure, along with its evolution under extended cycling, whereas energy density is not typically quoted. When simply comparing Si/Sn with graphite, for example, this is not a problem as these materials discharge at very similar, low voltages (0.1 - 0.7 V vs Li/Li^+).[33][34] However, when examining CAMs, which discharge in multiple steps over a wide voltage range, reporting gravimetric capacity alone is not sufficient as it treats capacities as equally valuable regardless of discharge voltage. Furthermore, the wide voltage range over which CAMs discharge is itself a barrier preventing their integration into existing battery technology due to much of the capacity being unusable due to unsuitable discharge voltages. For example, utilising an anode voltage range of 0 - 2.5 V vs Li/Li^+ corresponds to a range of approx. 3.9 - 1.4 V in a full cell *versus* a Lithium Cobalt Oxide (LCO) cathode, whereas current commercially available Li-ion batteries typically discharge over a higher and narrower voltage range, 3.5 – 3.7 V.[4],[35] This fact is often obfuscated by the testing of CAMs in half-cells alone, utilizing a Li foil reference/counter electrode, as opposed to also testing in full cells. The narrow focus on achieving the highest possible half cell gravimetric capacities leads to the design of materials which achieve this criterion alone, and ignores other, arguably more important, criteria (energy density, narrow discharge voltage range).

The contributions of the various lithiation/delithiation processes in a CAM are not typically analyzed individually but rather the sum total of gravimetric capacity is solely reported. This means that valuable insights into the sources of capacity, and the causes of capacity degradation under extended cycling, are therefore overlooked .[14,19,30–32]

These insights would prove useful in the design of new, more stable materials which maximize usable energy density.

Here we report a study in which the poor suitability of CTPs for prospective battery anode materials is highlighted. As an illustration, we perform a thorough analysis of a CAM, dicopper zinc tin sulfide (Cu_2ZnSnS_4) or CZTS. This material has achieved among the highest reported gravimetric capacities among CAMs,[30–32,36–39] and, notably, wide stoichiometric variations are possible, enabling modulation of the lithiation characteristics through facile synthetic techniques.[40,41] Furthermore, the multi-step nature of the lithiation/delithiation processes that occur over a wide voltage range during cycling of CZTS render it an ideal material with which to examine and compare these processes, and to illustrate the inadequate nature of CTPs. Here, the conversion and alloying processes are compared and contrasted in terms of their contribution to overall capacity/energy density and stability under extended cycling. Half cell and full cell studies are used to illustrate the limitations (and potentially misleading nature) of simple tests opposite Li foil. The issues highlighted by these studies are particularly prevalent for, but not limited to, CAMs. Finally, recommendations for new testing protocols are proposed, focussed on moving from simple analysis of lithiation characteristics to assessment of suitability for real-world applications. This methodology enables more realistic material analysis for a wide range of potential anode materials, and should provide researchers with a more meaningful basis for designing new materials. We illustrate this point by designing a variation of the CZTS material, in which usable energy density is enhanced.

Experimental Method

Chemicals. Copper (II) acetylacetonate (99.9 %), zinc acetate (99.99 %), tri-octylphosphine oxide (TOPO, 99 %), 1-octadecene (90 %), tert-dodecylmercaptan (t-ddt, 98.5 %), 1-dodecanethiol (1-ddt, 98 %), anhydrous hexane (95 %), ammonium sulfide (40 – 48 % in H_2O), and Li foil were purchased from Sigma Aldrich, tin (IV) acetate (98 %) from ACROS Organics, tetradecylphosphonic acid (TDPA, 99 %) from PCI Synthesis, LCO cathode tapes from NEI corporation and separator paper from Celgard.

CZTS Nanorod Synthesis. The nanorods were synthesised according to a previously published method.[42] Briefly, in a typical synthesis, 131 mg copper (II) acetylacetonate, 45.5 mg zinc acetate, 88.5 mg tin (IV) acetate and 676 mg TOPO were mixed in 5 mL 1-octadecene in a 3-neck flask. The flask was then evacuated for 30 min using a Schlenk line, after which they were exposed to an argon atmosphere. The temperature was ramped up to 270 °C, during which a 1 mL mixture of 7:1 t-ddt:1-ddt was injected into the flask at 155 °C. The solution immediately turned from dark green to clear yellow after the injection. The reaction was allowed to proceed for 30 mins after injection, before being naturally cooled to 100 °C and dispensed into a vial. To achieve Sn-rich rods, the precursor masses were altered to 111 mg copper (II) acetylacetonate and 95.1 mg tin (IV) acetate, while the others were kept constant.

Electrophoretic Deposition. The nanorods were then washed and deposited according to an altered method previously published.[43] Briefly, 50 mg tetradecylphosphonic acid (TDPA) was added to a 1 ml extract of the as-synthesised product, and sonicated for 5 mins. 1 ml isopropanol was added and the mixture was vortexed for approx. 5 s. The nanorods were then isolated by centrifugation at 4,000 rpm for 5 mins before being dried under a stream of argon and redispersed in 1 ml anhydrous hexane. The deposition bath was created by adding 0.2 ml of this to 5 ml anhydrous hexane. Two Cu foil plates held approx. 5 mm apart were immersed in the bath and a voltage of 300 V was applied using a high voltage power supply (TECHNIX SR-5-F-300), and monitored throughout deposition by a TTi 1604 Digital Multimeter. Deposition on the positive electrode was observed and film thickness could be controlled by varying the total immersion time. All battery electrodes utilised 0.1 - 0.2 mg cm^{-2} active material (precise masses were determined using a Sartorius SE2 ultra-microbalance, with a readability of 0.1 µg).

Ligand Removal. The resultant films typically included significant organic content in the form of the TDPA ligands. Removal of this material reduces inactive material and enhances film conductivity.[44],[45] This treatment was performed by immersing the electrodes in a 20mM solution of ammonium sulfide in methanol for 30 s, followed by rinsing in methanol. Typically, an 8x8 mm electrode gained approx. 15-25 µg during this treatment, due to formation of a thin copper sulfide film on the copper foil.

Characterization. Scanning electron microscopy (SEM) was performed with a Hitachi SU-70 system equipped with an Oxford Instruments Energy-Dispersive X-ray spectroscopy (EDS) detector, X-Ray diffraction (XRD) with a PANalytical X'Pert PRO MPD instrument with a Cu Kα radiation source (λ = 1.5418 A) with a 1-D X'celerator strip detector. Raman spectroscopy was carried out using a Horiba Labram 300 spectrometer system equipped with a 633nm laser.

Electrochemical Measurements. The electrochemical performance of the electrodes was evaluated by assembly of a Swagelok-type two-electrode cell in an Ar-filled glovebox. The electrodes were examined against either elemental Li (in a half cell configuration) or LCO (in a full cell configuration), with a Celgard separator placed between. LCO cathodes consisted of a 0.64cm^2 electrode on Al foil with a capacity of 555 µAh (implying a P:N ratio of 8.5 based on the theoretical capacity of CZTS). The electrolyte used for all tests was a 1 M solution of $LiPF_6$ in ethylene carbonate/diethyl carbonate (1:1 v/v, Sigma Aldrich) with 3 % vinylene carbonate (Sigma Aldrich) as an additive. Galvanostatic measurements were carried out using a Biologic MPG-2, and the cells were held at a temperature of 30 +/- 3 ºC. Specific lithiation processes were isolated by modulation of the upper and lower cutoff voltages during cycling. The cell capacities quoted in this work were determined based on the mass of NRs measured prior to ligand removal and thus these represent a small (5 – 10 %) underestimation of actual values.

Results and Discussion

Figure 1 shows the voltage profile of a half cell consisting of CZTS nanorods deposited on a Cu current collector opposite Li foil (SEM image in Figure S1).[42],[43] The material exhibited a multi-stage lithiation/delithiation with plateaus in 0.9 – 2.5 V range attributed to conversion processes involving the formation and deformation of sulfides (Equation 1),[36],[39] whereas the sub 0.9 V interactions consist of the formation/deformation of Li-Sn/Zn alloys (Equation 2 & 3). The initial reaction pathway is as follows:

$$Cu_2ZnSnS_4 + 8Li^+ + 8e^- \rightarrow 2Cu + Zn + 4Li_2S \quad (1) \quad 488mAh\,g^{-1}$$

$$Sn + 4.4Li^+ + 4.4e^- \rightarrow Li_{4.4}Sn \quad (2) \quad 268mAh\,g^{-1}$$

$$Zn + 1.5Li^{+} + 1.5e^{-} \rightarrow Li_{1.5}Zn \quad (3) \quad 91\ mAh\ g^{-1}$$

Based on the presence of multiple plateaus in the first delithiation, and a large change in electrochemical characteristics between the 1st and 2nd cycles,[30–32,39,46] it was concluded that the individual metal sulfides (Cu_2S, ZnS and SnS_2) rather than CZTS, were formed at this stage. In subsequent lithiations, the conversion process in equation 1 therefore separates into:

$$Cu_2S + 2Li \rightarrow 2Cu + Li_2S \quad (4)$$

$$SnS_2 + 4Li \rightarrow Sn + 2Li_2S \quad (5)$$

$$ZnS + 2Li \rightarrow Zn + Li_2S \quad (6)$$

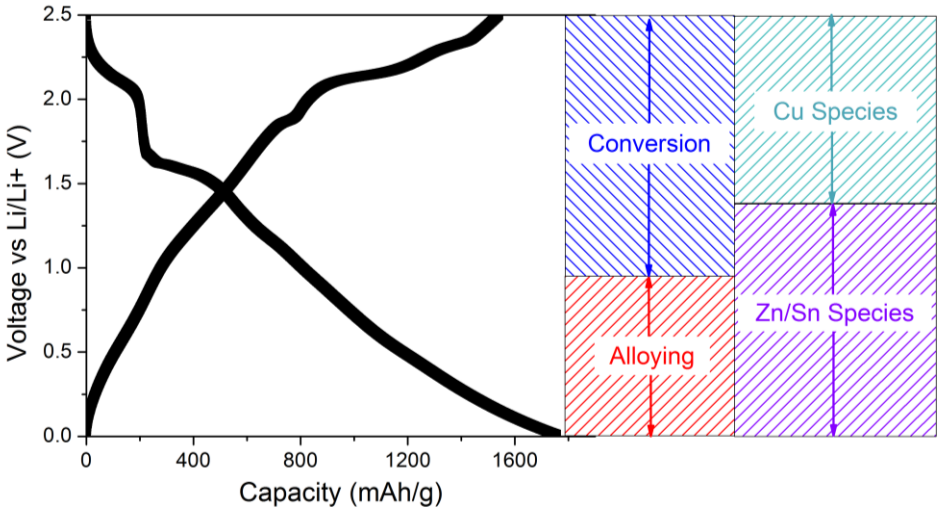

Figure 1: Voltage profile of CZTS half cell galvanostatically cycled at 200 mA g^{-1} (Cycle 2 is shown). The voltage range is separated by (i) lithiation process type, and (ii) the metal species involved. The observed extra capacity above theoretical was attributed to capacitive effects (known to occur for sulfide materials and other CAMs[18,47,48]), as well as the contribution from the $Cu_{2-x}S$ film formed during ligand removal. The contribution of this film has been previously demonstrated to be initially significant, but diminishes rapidly with cycling.[49]

All processes relating to the $Cu_{2-x}S$ portion of CZTS occur > 1.4 V (both lithiation and delithiation), and therefore processes observed < 1.4 V were attributed to Zn/Sn species. This voltage-separation of processes is useful as it enables their individual properties to be compared and contrasted in a facile manner within a single material. Firstly, processes were separated and analyzed based on the metal species involved. Two identical CZTS electrodes were prepared, and one was cycled initially at higher voltage between 1.4 – 2.5 V vs. Li/Li^+ ("Cell A") and the other initially at lower voltage between 0 – 1.4 V ("Cell B"). Figure 2a and b show the gravimetric capacities of these two electrodes. The initially high capacity of Cell A in Figure 2a (742 mAh g^{-1}) underwent a dramatic initial decay where capacities fell below 150 mAh g^{-1} after 10 cycles. Examination of the differential capacity plots (DCPs) for cycle 2 and 50 (Figure 2c) revealed initial anodic peaks at 1.87 V and 2.34 V, which shifted and reduced in intensity with cycling, confirming the high capacity but poor stability of the $Cu_{2-x}S$ conversion processes. After 575 cycles, the voltage range for Cell A was switched to 0 – 1.4 V *i.e.* the range in which the Zn and Sn species are electrochemically active. The capacity immediately increased above 400 mAh g^{-1}. Despite the very low capacity of Cell A under extended cycling, the Zn/Sn material remained electrically contacted to the current collector. After a further 376 low-voltage cycles, Cell A was cycled over the full range of 0 – 2.5 V for a final cycle and, remarkably, exhibited a discharge capacity of 1,420 mAh g^{-1}. This result confirms that the observed fading of battery capacity is recoverable under the right circumstances, and that the capacity losses encountered in both the high voltage and low voltage phases were not related to material delamination/disintegration or sulfide dissolution. This high capacity indicates that Li that had become "trapped" during the early stage cycling over 1.4 – 2.5 V, was brought back into measurement range by decreased overpotential. This was confirmed by the re-appearance of a large delithiation peak at 2.44 V in the DCP (Figure S2) during the final delithiation, which was the major contributor to the high capacity. Notably, it appears that the cycling over the lower voltage range was required in order to bring about this overpotential reduction, which suggests a synergistic effect of combined alloying and conversion processes.

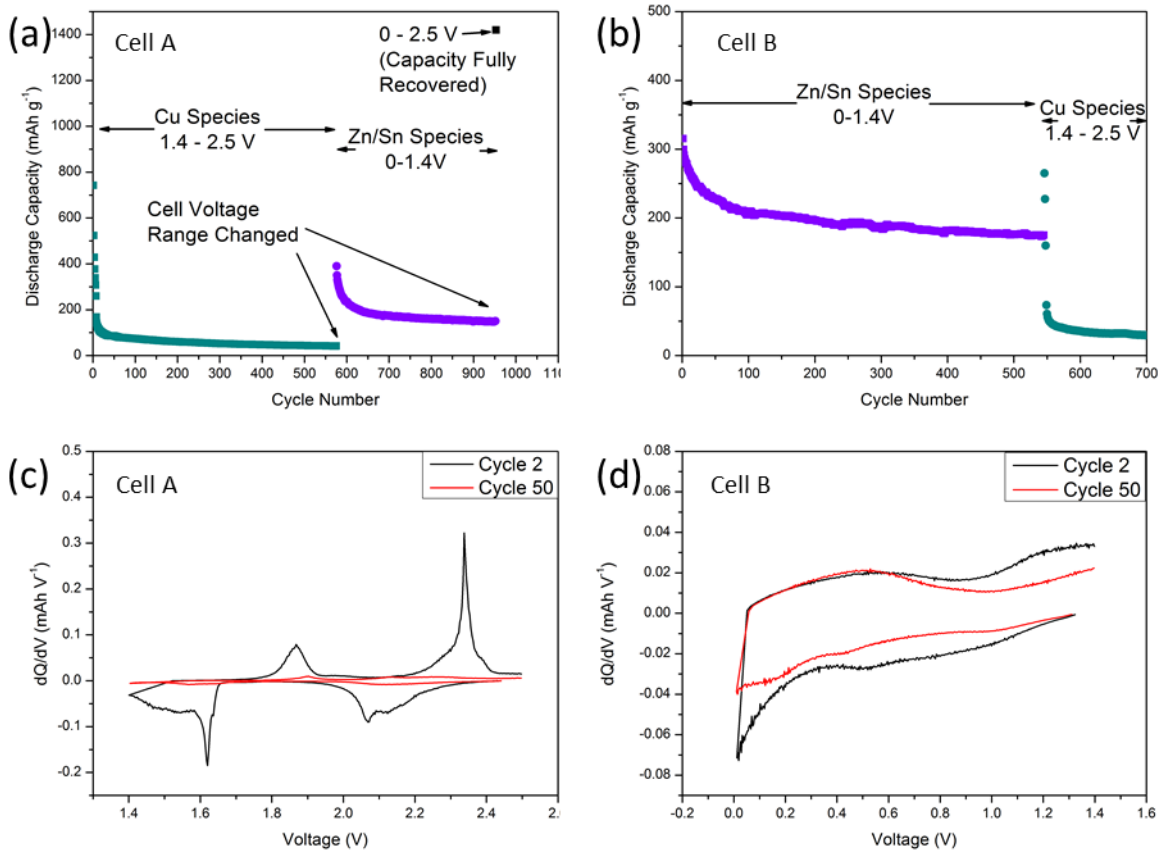

Figure 2: (a) and (b) show discharge capacities of CZTS half cells cycled at 200 mA g^{-1} in limited voltage ranges. Note that the voltage ranges were switched after approximately 550 cycles, as indicated on the plots. The DCPs for these two cells, showing cycles 2 and 50, are shown in (c) and (d).

In order to investigate the performance of the Sn and Zn-related processes alone, Cell B was tested at an initial low-voltage cycling stage, followed by a high voltage stage (Figure 2b). Cell B exhibited a lower initial capacity (315 mAh g^{-1}) than Cell A; however the stability under extended cycling was far superior. An initial decay over the first 100 cycles was followed by a stabilization period, in which the capacity faded by just 0.04 %/cycle (averaged over cycles 100 – 500). Upon switching the voltage range to 1.4 – 2.5 V, the capacity momentarily increased, before quickly falling to < 50 mAh g^{-1}, mirroring the initial cycles that were observed in this range for Cell A in Figure 2a. The DCPs for Cell B (Figure 2d) show that the initial capacity fade is almost entirely related to a reduction in capacity in the > 1 V region i.e. Zn/Sn conversion processes. Conversely, the alloying delithiation peak (~ 0.5 V)

is extremely stable, both in terms of position and intensity. This confirms the excellent reversibility of Li alloying with Zn/Sn (equation 2 and 3), but a significant degree of irreversibility of the associated sulfidation reactions (equation 5 and 6).

Given the high stability of the alloying processes in particular, it was useful to isolate these by further restricting the cycling voltage range. To that end, a third identical cell (Cell C) was cycled over the range 0 – 0.9 V at 200 mA g^{-1} (Figure 3). An initial discharge capacity of 317 mAh g^{-1} was observed, however the stability was notably superior to the wider voltage ranges. After a small decay which is related to SEI formation,[31,50,51] the rate of capacity fade was just 0.001 %/cycle (between cycles 100 – 1,000). This demonstrates the far superior capacity retention of the alloying process over conversion for CZTS. Furthermore, this level of long-term capacity retention is not typically observed for anodes consisting of elemental Sn or Zn.[34,52–55] The enhanced stability here is ascribed to the beneficial effect of the presence of non-cycling Li_2S/Cu buffer material.[12,19,23]

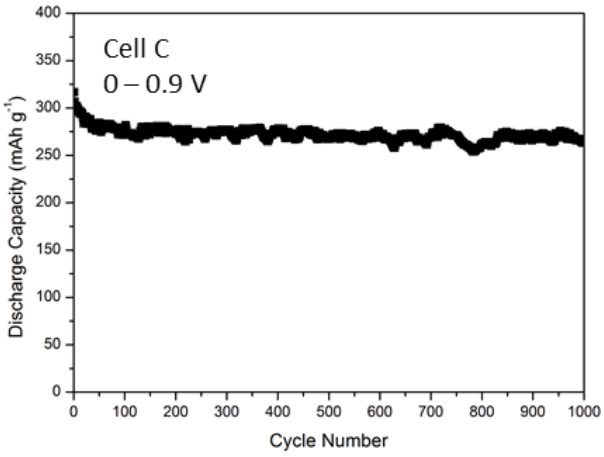

Figure 3: Gravimetric discharge capacity of CZTS half cell cycled between 0 – 0.9 V at 200 mA g^{-1}

The narrow range over which these alloying processes discharge is more suitable for incorporation into existing LIB full cells, which typically operate over a narrow range, 3.5 – 3.7 V.[4],[35] Furthermore, their discharge voltages are close to 0 V vs. Li/Li^+, thereby providing more energy density than the conversion processes. To illustrate this, it is useful to consider a hypothetical material with a single, constant-voltage discharge plateau with a capacity of

300 mAh g^{-1}. When used as an anode in a full cell opposite a hypothetical 3.9 V, 150 mAh/g cathode, this plateau contributes 340 Wh kg^{-1} if positioned at 0.5 V vs. Li/Li^+, as opposed to only 180 Wh kg^{-1} if at 2.1 V *vs.* Li/Li^+. It is therefore desirable for an anode material to (a) delithiate over a narrow voltage range, and (b) for this range to be situated at a low voltage vs. Li/Li^+. It can then be concluded that reporting the gravimetric capacity of a material over a wide voltage range (e.g. 0 – 2.5 V *vs.* Li/Li^+) is useful for investigating its lithiation characteristics, however this cannot be considered a meaningful assessment of its potential as a LIB anode. While this is particularly prevalent in the case of CAMs (binary, ternary and quaternary) due to their multi-step lithiation nature, it is also applicable to single mode materials with relatively high discharge voltages such as Cu_xS (discharges at 1.5 - 2 V *vs.* Li/Li^+[9]) or NiS_x (discharges at ~ 1.9 – 2.1 V *vs.* Li/Li^+[56]) which have been proposed as potential anodes.[9,47,56,57]

It should be noted that while the simple calculation above will provide an estimate of full cell energy density from half cell gravimetric capacity data alone, this is rarely reported. Furthermore, full cells measurements can divert significantly from half cell measurements (particularly during long-term cycling), due to e.g. limited Li availability or an evolution in cathode voltage.[58] Given the ready availability of standard commercial cathode electrodes, full cell measurements should not represent a significant extra amount of work for researchers.

To demonstrate this in the context of a CAM, CZTS electrodes were cycled at 200 mA g^{-1} (anode active mass basis) in full cell configurations *i.e.* a 2-electrode cell utilizing a LCO electrode as the cathode. Three voltage ranges were tested, (i) 3.9 – 1.4 V (includes all processes), (ii) 3.9 – 2.5 V (Zn/Sn species only), and (iii) 3.9 – 3.0 V (Zn/Sn alloying processes only). Here it is useful to introduce the concept of "usable capacity/energy", defined as that which is discharged > 3 V in a full cell *vs.* LCO. Only energy available in this region satisfies the requirement of high, constant-output voltage. This criterion effectively allows alloying but disallows conversion processes in CAMs. Electrochemical analysis of full cells cycled over three voltage ranges is shown in Figure 4.

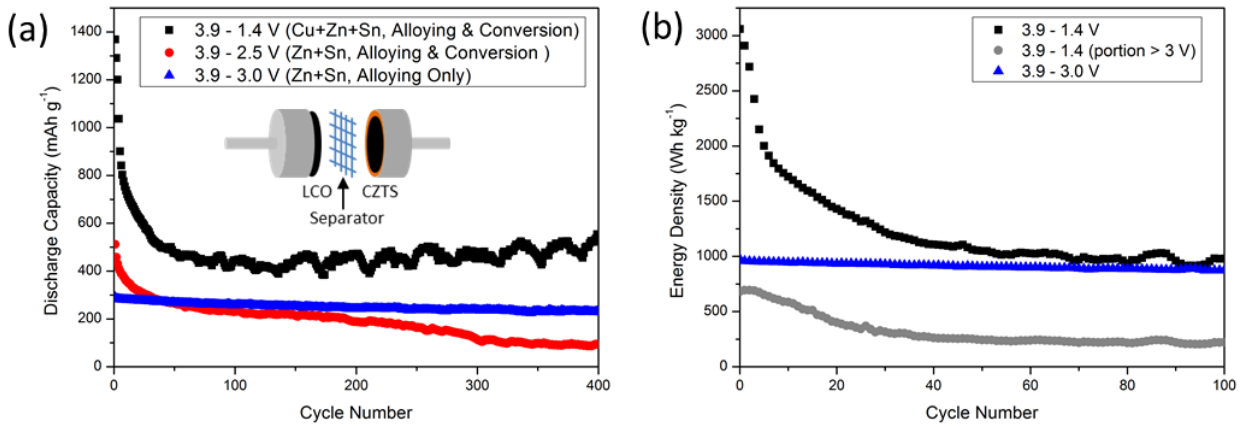

Figure 4: (a) Gravimetric capacity (anode basis) of CZTS anodes cycled at 200 mA g^{-1} in a full cell configuration utilizing an LCO cathode, over varying voltage ranges. Inset in (a) is a schematic showing the full cell structure. (b) Energy density (based on anode mass alone) of full cells. For the 3.9 – 1.4 V cell, shown are both the total energy density (black) and the usable energy density i.e. that occurring > 3 V (grey). Energy density values based on the combined anode plus cathode mass are provided in Figure S3. The 3.9 – 1.4 V gravimetric capacity data (black curve in Figure 4a) was reported as part of a previous publication,[46] and is included here to enable comparison with the other voltage ranges.

The initial high gravimetric capacity of the 3.9 – 1.4 V full cell fell dramatically over the first 100 cycles, before entering a period of gradual recovery, exhibiting a capacity of 555 mAh g^{-1} after 400 cycles. In contrast, the 3.9 – 3.0 V range cell exhibited a lower initial capacity of 291 mAh g^{-1} (similar to that of the equivalent half cell in Figure 3) but excellent stability, with a capacity fade rate of just 0.02 %/cycle (averaged over cycle 100 – 1,000, see Figure S4 and S5 for further extended cycling data and DCPs). Notably, the temperature-related sinusoidal effect observed in the capacity trends of the 3.9 – 1.4 V cell in Figure 4a was not present for the 3.9 – 3.0 V cell cycled over the same timeframe. This indicates that the conversion processes had a higher susceptibility to detrimental temperature-related effects on capacity than alloying.

It may be expected that, given the limited reversibility of the Zn/Sn conversion reactions, the capacity of the 3.9 – 2.5 V cell would converge with that of the 3.9 – 3.0 V cell under extended cycling. However, the capacity in fact

fell below that of the 3.9 – 3.0 V cell after 47 cycles, and subsequently continued to decrease. This indicates that not only are the Zn/Sn conversion processes less stable, their inclusion in cycling actually reduces the stability of the corresponding alloying processes. The proposed "buffer" role of Li_2S is well reported,[12,19,23] however to our knowledge no studies of the effect of continued formation and deformation of this Li_2S have been carried out. In fact, standard testing procedures in existing studies of CAMs involve simply extended cycling over the entire voltage, encompassing all mechanisms/processes.[14,30,59,60] The lower stability of the 3.9 – 2.5 V cell here indicates that this standard procedure is not optimum for extracting maximum capacity, and may in fact be significantly underestimating the capacity retention capabilities of CAMs.

Nevertheless, by comparison of full cell gravimetric capacities alone, the widest voltage range (3.9 – 1.4 V) appears to demonstrate a clear advantage. However, to account for the varying voltage ranges, the energy density is a superior metric with which to assess performance. A comparison of the energy densities of the full cells is shown in Figure 4b. While the stabilized gravimetric capacity of the 3.9 - 1.4 V range is 73% higher than the 3.9 – 3.0 V range at cycle 100 (445 mAh g^{-1} vs. 257 mAh g^{-1}, Figure 4a), much of this excess capacity is output at a lower, less useful, voltage. When the *energy densities* at cycle 100 are instead compared, this advantage is reduced to just 13% (992 Wh kg^{-1} *vs.* 877 Wh kg^{-1}, based on anode mass only). Furthermore, the usable energy density of the 3.9 – 1.4 V cell (225 Wh kg^{-1}) is in fact significantly lower than that of the 3.9 – 3.0 V cell. This result again indicates that the conversion processes are not only themselves unstable, but also that cycling in the conversion range has a detrimental effect on the overall stability of the electrode. It can therefore be concluded that cycling only in the 3.9 – 3.0 V range is optimal for maximum usable energy density extraction while benefitting from the stability provided by the presence of non-cycling Li_2S. Such operation in the alloying regime alone would necessitate a pre-lithiation step to complete the conversion reaction (forming alloy metal + Li2S) to avoid the necessity for a large cathode excess.

The greater stability and energy density of the alloyed process in these combined-mode materials, as well as the identification of usable energy density as the most important parameter, enables significant optimization of material

composition. In the case of CZTS, an increase of the Sn content achieves this. To demonstrate this, the stoichiometry of the material was modified to a Sn-rich/Cu-poor formulation (EDS indicated $Cu_{1.7}Zn_{1.1}Sn_{1.2}S_4$, see Figure S6). This effectively exchanged some high voltage capacity for low voltage capacity, increasing the alloying portion at the expense of conversion. The use of wurtzite CZTS as the model material is key here, as the cationic sites in crystals of this phase are interchangeable,[40],[41] and therefore large variations in stoichiometry are achievable.

These Sn-rich nanorods were processed into half cells as before and galvanostatically cycled from 0 - 1.4 V vs. Li/Li^+ to again include the Zn/Sn processes but exclude Cu-related ones. Results are shown in Figure 5a. The initial capacity of the Sn-rich variation, at 426 mAh g^{-1}, was 35% higher than that of the stoichiometric CZTS. Crucially the stability trend was identical, and the capacity advantage was maintained at 37% after 200 cycles. Figure 5b compares DCPs for the 2 nanorod variants over their first lithiation, and shows a decrease in intensity of the anodic 1.7 V peak and an increase in intensity of the 1.1 V peak when a Sn-rich formulation is utilized, indicating that the higher voltage peak is, as was assumed, largely Cu- related, whereas the lower is largely Sn-related. The sub 1 V peaks are also more intense in the Sn-rich sample.

A significant enhancement of usable capacity by facile material alteration confirms the advantage of testing protocols that value reporting of this more meaningful parameter over simply raw gravimetric capacity. It is important to note that a comparison of the two stoichiometries over 0 – 2.5 V (as per CTPs) would obscure the benefit of the Sn-rich formulation, due to the reduction in high voltage capacity cancelling out the gains in low voltage capacity.

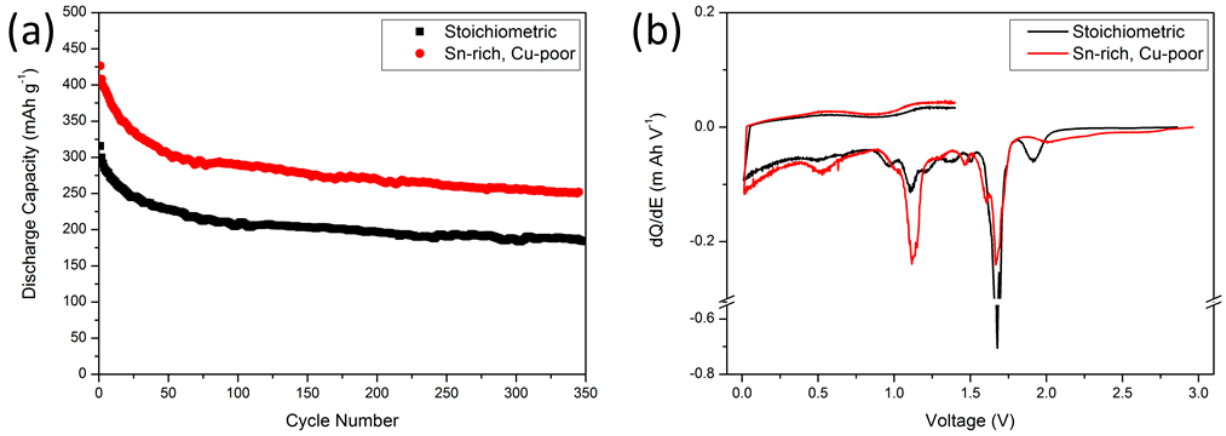

Figure 5: (a) Gravimetric capacity of CZTS nanorods as a function of cycle number for both stoichiometric and Sn-rich variants, cycled at 200 mA g^{-1} over 0 – 1.4 V. (b) DCP of the first cycle for the two variant

Conclusions

CTPs carried out on new battery anode materials omit several important parameters and are unsuitable for a true assessment of materials that discharge in multiple steps, at a high voltage vs Li/Li^+, or over a wide voltage range. This is particularly important for CAMs, which often exhibit delithiation processes from 0 to 2.5 V *vs.* Li/Li^+. To address these issues, we recommend the adoption of a new testing protocol, in which total and usable full cell energy density are necessarily reported alongside gravimetric capacity. Furthermore, we recommend individual analysis of lithiation processes in CAMs, as significant variations in capacity and particularly stability were observed for processes in a model system, CZTS. This type of analysis showed that the true advantage of CAMs lies in the energy density provided by the alloying processes, and the stability provided by the Li_2S buffer where this stability effect was maximized when the Li_2S is not cycled. In this way, CTPs currently overestimate usable capacity while potentially underestimating capacity retention. The adoption of this protocol would lead to a more meaningful assessment of new anode materials, as well as enabling significant material optimization which is obscured by current protocols.

Author Information

Corresponding Author

* Kevin.m.ryan@ul.ie

Author Contributions

The manuscript was written through contributions of all authors. All authors have given approval to the final version of the manuscript.

Notes

The authors declare no competing financial interest.

Funding Sources

The authors would like to acknowledge Science Foundation Ireland (SFI) Grant No. 11-PI-1148 for funding this research.

Supporting Information

Supporting Information is available from the Wiley Online Library or from the author.

REFERENCES

[1] V. Aravindan, Y. Lee, S. Madhavi, *Adv. Energy Mater.* **2015**, 1402225.

[2] M. N. Obrovac, V. L. Chevrier, *Chem. Rev.* **2014**, 11444–11502.

[3] K. Cao, T. Jin, L. Jiao, *Mater. Chem. Front.* **2017**, *1*, 2213–2242.

[4] N. Nitta, F. Wu, J. T. Lee, G. Yushin, *Mater. Today* **2015**, *18*, 252–264.

[5] K. Stokes, H. Geaney, G. Flynn, M. Sheehan, T. Kennedy, K. M. Ryan, *ACS Nano* **2017**, 10088–10096.

[6] B. Wang, B. Luo, X. Li, L. Zhi, *Mater. Today* **2012**, *15*, 544–552.

[7] M. Armand, *Nature* **2001**, *414*, 359–367.

[8] Y. Kim, J. B. Goodenough, *J. Phys. Chem. C* **2008**, *112*, 15060–15064.

[9] X. Li, X. He, C. Shi, B. Liu, Y. Zhang, S. Wu, Z. Zhu, J. Zhao, *ChemSusChem* **2014**, *7*, 3328–3333.

[10] X. Zuo, J. Zhu, P. Müller-buschbaum, Y. Cheng, *Nano Energy* **2017**, *31*, 113–143.

[11] B. Jerliu, R. Steitz, V. Oberst, U. Geckle, M. Bruns, H. Schmidt, *J. Phys. Chem. C* **2014**, *118*, 9395–9399.

[12] D. Bresser, S. Passerini, B. Scrosati, *Energy Environ. Sci.* **2016**, *9*, 3348.

[13] X. Rui, H. Tan, Q. Yan, *Nanoscale* **2014**, *6*, 9889–9924.

[14] Z. Zhang, C. Zhou, M. Jia, Y. Fu, J. Li, Y. Lai, *Electrochim. Acta* **2014**, *143*, 305–311.

[15] P. Chen, Y. Su, H. Liu, Y. Wang, *ACS Appl. Mater. Interfaces* **2013**, 12073–12082.

[16] H. Tao, S. Zhu, X. Yang, L. Zhang, S. Ni, *J. Electroanal. Chem.* **2016**, *760*, 127–134.

[17] Z. Zhang, Y. Fu, C. Zhou, J. Li, Y. Lai, *Solid State Ionics* **2015**, *269*, 62–66.

[18] D. Bhattacharjya, A. Sinhamahapatra, J.-J. Ko, J.-S. Yu, *Chem. Commun.* **2015**, *51*, 13350–13353.

[19] J. Lin, J. Lim, D. H. Youn, K. Kawashima, J. Kim, H. Guo, G. Henkelman, A. Heller, C. B. Mullins, *ACS Nano* **2017**, *11*, 10347–10356.

[20] Z. Wei, L. Wang, M. Zhuo, W. Ni, H. Wang, J. Ma, *J. Mater. Chem. A* **2018**, DOI 10.1039/C8TA02695E.

[21] Y. Kim, H. Hwang, K. Lawler, S. W. Martin, J. Cho, *Electrochim. Acta* **2008**, *53*, 5058–5064.

[22] T. Kim, C. Kim, D. Son, M. Choi, B. Park, *J. Power Sources* **2007**, *167*, 529–535.

[23] H. S. Im, Y. J. Cho, Y. R. Lim, C. S. Jung, D. M. Jang, J. Park, F. Shojaei, H. S. Kang, *ACS Nano* **2013**, *7*, 11103–11111.

[24] H. Senoh, T. Takeuchi, H. Kageyama, H. Sakaebe, *J. Power Sources* **2010**, *195*, 8327–8330.

[25] A. M. Tripathi, S. Mitra, *RSC Adv.* **2014**, 10358–10366.

[26] Y. Zeng, H. Li, B. Qu, B. Xiang, L. Wang, Q. Zhang, Q. Li, T. Wang, Y. Wang, *CrystEngComm* **2012**, *14*, 550–554.

[27] Z. Zhang, C. Zhou, Y. Liu, J. Li, Y. Lai, M. Jia, *Int. J. Electrochem. Sci.* **2013**, *8*, 10059–10067.

[28] Z. Zhang, Y. U. N. Fu, C. Zhou, Y. Lai, *J. Electron. Mater.* **2015**, *44*, 252–257.

[29] X. Tang, X. Yao, Y. Chen, B. Song, D. Zhou, J. Kong, C. Zhao, X. Lu, *J. Power Sources* **2014**, *257*, 90–95.

[30] J. Chiu, T. Chou, D. P. Wong, Y. Lin, C. Shen, S. Hy, Y. Tai, H. Wu, K. Chen, *Nano Energy* **2018**, *44*, 438–446.

[31] Q. Jiang, X. Chen, H. Gao, C. Feng, Z. Guo, *Electrochim. Acta* **2016**, *190*, 703–712.

[32] J. Lin, J. Guo, C. Liu, H. Guo, *ACS Appl. Mater. Interfaces* **2016**, *8*, 34372–34378.

[33] G. Kim, T. Kennedy, M. Brandon, H. Geaney, K. M. Ryan, S. Passerini, G. B. Appetecchi, **2017**, DOI 10.1021/acsnano.7b01705.

[34] D. Zhou, W. Song, X. Li, L. Fan, Y. Deng, *J. Alloys Compd.* **2017**, *699*, 730–737.

[35] L. W. Hruska, *Twelfth Annu. Batter. Conf. Appl. Adv. Long Beach, CA* **1997**, 205–210.

[36] X. Yang, J. Xu, L. Xi, Y. Yao, Q. Yang, C. Y. Chung, C.-S. Lee, *J. Nanoparticle Res.* **2012**, *14*, 931.

[37] J. Li, J. Shen, Z. Li, X. Li, Z. Sun, Z. Hu, S. Huang, *Mater. Lett.* **2013**, *92*, 330–333.

[38] W.-H. Zhou, Y.-L. Zhou, J. Feng, J.-W. Zhang, S.-X. Wu, X.-C. Guo, X. Cao, *Chem. Phys. Lett.* **2012**, *546*, 115–119.

[39] J. Lin, J. Guo, C. Liu, H. Guo, *ACS Appl. Mater. Interfaces* **2015**, *7*, 17311–17317.

[40] X. Lu, Z. Zhuang, Q. Peng, Y. Li, *Chem. Commun.* **2011**, *47*, 3141–3143.

[41] G. Bree, C. Coughlan, H. Geaney, K. M. Ryan, *ACS Appl. Mater. Interfaces* **2018**, *10*, 7117–7125.

[42] A. Singh, H. Geaney, F. Laffir, K. M. Ryan, *J. Am. Chem. Soc.* **2012**, *134*, 2910–2913.

[43] P. Liu, S. Singh, G. Bree, K. M. Ryan, *Chem. Commun.* **2016**, *52*, 2–5.

[44] O. O. Otelaja, D. H. Ha, T. Ly, H. Zhang, R. D. Robinson, *ACS Appl. Mater. Interfaces* **2014**, *6*, 18911–18920.

[45] H. Zhang, B. R. Hyun, F. W. Wise, R. D. Robinson, *Nano Lett.* **2012**, *12*, 5856–5860.

[46] G. Bree, H. Geaney, K. Stokes, K. M. Ryan, *J. Phys. Chem. C* **2018**, *122*, 20090–20098.

[47] P. Fan, H. Liu, L. Liao, J. Fu, Z. Wang, G. Lv, L. Mei, H. Hao, J. Xing, J. Dong, *RSC Adv.* **2017**, *7*, 49739–49744.

[48] L. Croguennec, M. R. Palacin, *J. Am. Chem. Soc.* **2015**, *137*, 3140–3156.

[49] D. H. Ha, T. Ly, J. M. Caron, H. Zhang, K. E. Fritz, R. D. Robinson, *ACS Appl. Mater. Interfaces* **2015**, *7*, 25053–25060.

[50] M. B. Pinson, M. Z. Bazant, *J. Electrochem. Soc.* **2013**, *160*, A243–A250.

[51] E. Peled, S. Menkin, *J. Electrochem. Soc.* **2017**, *164*, A1703–A1719.

[52] M. Wu, X. Li, Q. Zhou, H. Ming, J. Adkins, J. Zheng, *Electrochim. Acta* **2014**, *123*, 144–150.

[53] C. Liu, H. Huang, G. Cao, F. Xue, R. Alberto, P. Camacho, X. Dong, *Electrochim. Acta* **2014**, *144*, 376–382.

[54] L. Liu, F. Xie, J. Lyu, T. Zhao, T. Li, B. Gill, *J. Power Sources* **2016**, *321*, 11–35.

[55] T. Fujieda, S. Takahashi, S. Higuchi, *J. Power Sources* **1992**, *40*, 283–289.

[56] A. A. Abdelhamid, X. Yang, J. Yang, X. Chen, J. Y. Ying, *Nano Energy* **2016**, *26*, 425–437.

[57] M. Zhou, N. Peng, Z. Liu, Y. Xi, H. He, Y. Xia, *J. Power Sources* **2016**, *306*, 408–412.

[58] G.-H. Lee, S.-J. Kim, M.-C. Kim, H.-S. Choe, D.-M. Kim, S.-B. Han, D.-H. Kwak, J. H. Jeong, K.-W. Park, *RSC Adv.* **2016**, *6*, 92259–92266.

[59] B. Qu, H. Li, M. Zhang, L. Mei, L. Chen, Y. Wang, Q. Li, T. Wang, *Nanoscale* **2011**, *3*, 4389.

[60] X. Yin, C. Tang, M. Chen, S. Adams, H. Wang, H. Gong, *J. Mater. Chem. A* **2013**, *1*, 7927.

10.1002/celc.201800990